PNAS RESEARCH ARTICLE | PHYSIOLOGY

A TRPM7 mutation linked to familial trigeminal neuralgia: Omega current and hyperexcitability of trigeminal ganglion neurons

Roberta Gualdani[a], Philippe Gailly[a], Jun-Hui Yuan[b,c,1], Xavier Yerna[a], Giulia Di Stefano[d], Andrea Truini[d], Giorgio Cruccu[d], Sulayman D. Dib-Hajj[b,c], and Stephen G. Waxman[b,c,2]

Edited by Bruce Bean, Harvard Medical School, Boston, MA; received October 27, 2021; accepted August 3, 2022

Trigeminal neuralgia (TN) is a unique pain disorder characterized by intense paroxysmal facial pain within areas innervated by the trigeminal nerve. Although most cases of TN are sporadic, familial clusters of TN suggest that genetic factors may contribute to this disorder. Whole-exome sequencing in patients with TN reporting positive family history demonstrated a spectrum of variants of ion channels including TRP channels. Here, we used patch-clamp analysis and Ca^{2+} and Na^{+} imaging to assess a rare variant in the TRPM7 channel, p.Ala931Thr, within transmembrane domain 3, identified in a man suffering from unilateral TN. We showed that A931T produced an abnormal inward current carried by Na^{+} and insensitive to the pore blocker Gd^{3+}. Hypothesizing that replacement of the hydrophobic alanine at position 931 with the more polar threonine destabilizes a hydrophobic ring, near the voltage sensor domain, we performed alanine substitutions of F971 and W972 and obtained results suggesting a role of A931-W972 hydrophobic interaction in S3-S4 hydrophobic cleft stability. Finally, we transfected trigeminal ganglion neurons with A931T channels and observed that expression of this TRPM7 variant lowers current threshold and resting membrane potential, and increases evoked firing activity in TG neurons. Our results support the notion that the TRPM7-A931T mutation located in the S3 segment at the interface with the transmembrane region S4, generates an omega current that carries Na^{+} influx in physiological conditions. A931T produces hyperexcitability and a sustained Na^{+} influx in trigeminal ganglion neurons that may underlie pain in this kindred with trigeminal neuralgia.

TRP channels | human mutations | gating current | trigeminal neuralgia

Significance

This study explores the potential pathogenic effects of a novel mutation of TRPM7 channel (A931T) identified in a 73-year-old man affected by familial trigeminal neuralgia. We show that A931T results in an abnormal Na^{+} influx that is carried by an omega current and appears to be due to destabilization of a hydrophobic interaction between S3 and S4 transmembrane domains. We demonstrate that the expression of TRPM7 mutant channels depolarizes membrane potential of trigeminal ganglion neurons and increases their hyperexcitability that may contribute to trigeminal neuralgia in patients carrying this mutation.

Trigeminal neuralgia (TN) is a unique neuropathic facial pain disorder characterized by severe unilateral paroxysmal pain, triggered by usually innocuous mechanical stimuli such as light touch (1). In most patients, TN occurs in the context of neurovascular compression of the trigeminal nerve; nevertheless, some individuals display neurovascular compression without developing TN, and in a significant number of TN patients, no apparent cause of trigeminal nerve disturbance can be found. In these patients, it has been suggested that genetic factors may contribute to the pathophysiology of TN. This hypothesis is suggested by the earlier age of onset of TN in patients without vascular compression of the trigeminal nerve (2) and the demonstration that TN can occur in a familial manner (3). Abnormal hyperexcitability of trigeminal ganglion neurons has been identified as a factor that contributes to pain in trigeminal neuralgia (4–6). In a recent cross-sectional study (7), whole exome sequencing of the electrogenisome of trigeminal ganglion of a large cohort of patients reporting a TN-positive familial history revealed 41 rare variants in ion channels, including mutations in voltage-gated sodium channels, chloride channels, calcium channels, transient receptor potential (TRP) channels, and gap junction channels. Among these variants, we previously analyzed a mutation of the cold receptor TRPM8, R30Q, found in a 61-y-old woman patient with a typical picture of TN and two affected brothers. We showed that the R30Q mutation in TRPM8 produces multiple gain-of-function changes in the channel. Specifically, the mutation enhanced channel activation; basal current amplitude, intracellular $[Ca^{2+}]$, and the response to the agonist menthol were increased in cells carrying the mutant channel (8).

In the present study, we analyzed a novel mutation of TRPM7 channel (A931T). This rare variant was identified in a 73-y-old man affected by TN, whose father was also affected. TN started with purely paroxysmal pain and, after an interval of 9 y without any symptoms, the patient developed concomitant continuous pain. TRPM7 is one of the TRP channels most highly expressed in dorsal root ganglia and trigeminal ganglion

Author affiliations: [a]Institute of Neuroscience, Université catholique de Louvain, B-1200 Brussels, Belgium; [b]Department of Neurology, Yale School of Medicine, New Haven, CT 06520; [c]Center for Neuroscience and Regeneration Research, Veterans Affairs Connecticut Healthcare, West Haven, CT 06515; and [d]Department of Human Neuroscience, Sapienza University, 00185 Rome, Italy

Author contributions: R.G., P.G., S.D.D.-H., and S.G.W. designed research; R.G., P.G., X.Y., S.D.D.-H., and S.G.W. performed research; P.G., S.D.D.-H., and S.G.W. contributed new reagents/analytic tools; R.G., P.G., X.Y., S.D.D.-H., and S.G.W. analyzed data; and R.G., P.G., J.-H.Y., G.D., A.T., G.C., S.D.D.-H., and S.G.W. wrote the paper.

The authors declare no competing interest.

This article is a PNAS Direct Submission.

[1]Present address: Department of Neurology and Geriatrics, Kagoshima University Graduate School of Medical and Dental Sciences, Kagoshima City, Kagoshima 890-8520, Japan.

[2]To whom correspondence may be addressed. Email: stephen.waxman@yale.edu.

This article contains supporting information online at http://www.pnas.org/lookup/suppl/doi:10.1073/pnas.2119630119/-/DCSupplemental.

Published September 12, 2022.

neurons (9), but in contrast to TRPM8, its function in the sensory system is not yet well established. TRPM7 is a ubiquitously distributed ion channel that belongs to the melastatin-related transient receptor potential (TRPM) ion channel subfamily, and is unique, together with TRPM6, in being both an ion channel and a protein kinase (10). It is an essential gene involved in the fine-tuning of cellular Mg^{2+} homeostasis and diseases caused by altered Mg^{2+} absorption (11). Moreover, its knockout results in block of cellular viability (12) and early embryonic lethality in mice (13, 14). TRPM7 is permeable to Mg^{2+} and Ca^{2+} (14), as well as to some toxic divalent cations (15). Moreover, TRPM7 is activated by depletion of intracellular MgATP and Mg^{2+}, with an IC_{50} of around 0.6 mM which is close to the physiological concentration of intracellular Mg^{2+} (16). As a consequence, the inward current amplitude generated by TRPM7 activation may be very small under physiological internal Mg^{2+} levels in the native cells but its enhancement may likely have pathological consequences.

In the present study, we explored the biophysical properties of the A931T mutation of the TRPM7 channel and assessed the effect of this mutation on excitability of trigeminal ganglion neurons. We show that A931T results in an abnormal Na^+ influx carried not through the canonical central pore of the channel, but rather by an omega current, and show that TRPM7 mutation produces trigeminal ganglion neuron hyperexcitability.

Results

A931T Mutation Massively Increases TRPM7 Inward Current. The heterozygous missense variant c.2791G > A results in the substitution of hydrophobic alanine to polar and hydrophilic threonine at p.931 in transmembrane domain 3 of the TRPM7 channel (p. Ala931Thr) (Fig. 1*A*). Human embryonic kidney (HEK) 293 cells were transiently transfected with plasmids encoding hTRPM7 wild-type (WT) and A931T and green fluorescent protein (GFP)-positive cells were analyzed by patch-clamp experiments. In a set of experiments WT and A931T were cotransfected (WT+A931T, 1:1) to model the heterozygous state of the patient. Whole-cell currents were elicited by a voltage ramp protocol ranging from −100 to +100 mV. After establishing the whole-cell configuration, TRPM7 currents were rapidly activated and reached a near plateau after ∼200–300 s (Fig. 1 *B–D*). TRPM7 channels were activated by depletion of intracellular Mg^{2+} due to intracellular perfusion of a Mg^{2+}-free pipette solution buffered with high concentration of EGTA. The WT current-voltage (I-V) relationships exhibited the hallmark biophysical features of hTRPM7, such as large outward current at positive potentials and small inward currents at negative voltages, a pronounced rectification, and a reversal potential near 0 mV, as expected for a nonselective Ca^{2+} channel (Fig. 1*B*). In these ionic conditions TRPM7 inward current is almost exclusively carried by Mg^{2+} and Ca^{2+}, while outward current is carried by the major internal monovalent cation Cs^+.

The A931T mutant produced dramatic changes in channel properties (Fig. 1*C*). Expression of A931T mutant resulted in a significantly larger inward current compared to WT (–3.5 ± 2.4 pA for WT, –53.8 ± 15.8 pA for A931T), whereas the outward currents of both clones were not statistically different. In vitro cotransfections of WT and A931T (WT+A931) revealed a rectification pattern similar to the mutant expressed alone (Fig. 1*D*), with an inward current density significantly greater than the mean WT current (–50.8 ± 16.7 pA for WT+A931T). The average outward and inward current densities obtained for WT, A931T, and WT+A931T transfected cells are summarized in Fig. 1*E*.

The ratio of outward currents measured at +80 mV to inward currents measured at –80 mV, the so-called rectification index (RI), of WT was 18 times larger than A931T and 12 times larger than WT+A931T (Fig. 1*F*). The A931T value of RI near 1 indicates that mutation results in loss of outward rectification. To further characterize the voltage sensitivity of A931T mutation, we recorded steady-state evoked currents during voltage steps from –200 mV to +200 mV from a holding potential of 0 mV. The steady-state I-V response for each cell was fitted by a Boltzmann distribution to estimate the $V_{1/2}$, slope factor k, maximal conductance G_{max} (Fig. 1*G*). The midpoint for activation was right shifted by ∼15 mV for A931T mutant compared with WT (WT, 87 ± 2 mV; A931T, 105 ± 5 mV, $P < 0.001$, unpaired Student's *t* test). Analysis of normalized conductance (G/G_{max}) revealed that the shape of G-V curve was significantly affected by A931T mutation: while WT and A931T normalized conductance followed a sigmoidal shape at depolarizing potentials, an additional conductance component appeared for A931T at around –60 mV, increased at hyperpolarizing potentials and saturated at around –180 mV. We carried out patch clamp experiments on cells expressing hTRPM7 WT and A931T, after replacing Cs^+ with K^+ in both extracellular and intracellular solutions to mimic physiological conditions (*SI Appendix*, Fig. S1). Our results showed that the current developed through WT and A931T in the presence of K^+ instead of Cs^+ was similar to the current traces shown in Fig. 1. More specifically, A931T expression, in the presence of K^+, resulted in a significantly larger inward current compared to WT, and this current was blocked by the specific TRPM7 antagonist NS8395 (17).

A931T Inward Current Is Blocked by NS8395 but Is Less Sensitive to Gd^{3+} Blockade and Naltriben Activation. In order to exclude the possibility that the current recorded from A931T might be due to some nonspecific leak current and to further confirm that the inward current observed in the mutant is due to TRPM7 activation, we perfused NS8593 and recorded whole-cell current from cells expressing WT, A931T, and WT+A931T. NS8593 at concentration of 10 μM blocked WT, A931T, and WT+A931T currents (Fig. 2 *A–C*), causing complete inhibition of both outward and inward currents. Thereafter, we recorded WT, A931T, and WT+A931T currents in the presence of the trivalent cation gadolinium (Gd^{3+}) (Fig. 2 *D–F*), a pore blocker of some voltage-gated Ca^{2+} channels, mechanosensitive Ca^{2+} channels, and TRP channels (18, 19). Enlarged view of the inward current traces in the presence and absence of Gd^{3+} is shown in Fig. 2*G*. We found that Gd^{3+}, similarly to NS8593, completely inhibited WT-mediated outward (+80 mV) and inward (–80 mV) currents (Fig. 2*H*). Gd^{3+} also completely blocked the outward currents of the mutant A931T and WT+ A931T (Fig. 2 *I* and *J*; filled blue bars; +80) but surprisingly it reduced the inward currents by only 19% and 9%, respectively (Fig. 2 *I* and *J*; open blue bars; –80). Current amplitudes not normalized before and after the application of the two inhibitors are reported in *SI Appendix*, Fig. S2.

Taken together, these findings indicate that the Gd^{3+}-insensitive A931T-mediated inward current, also in the heterozygous condition, was generated by the permeation of ions through a pathway distinct from the canonical central pore of the channel.

In order to further distinguish pharmacologically between the pore and the omega currents we studied in detail the effect

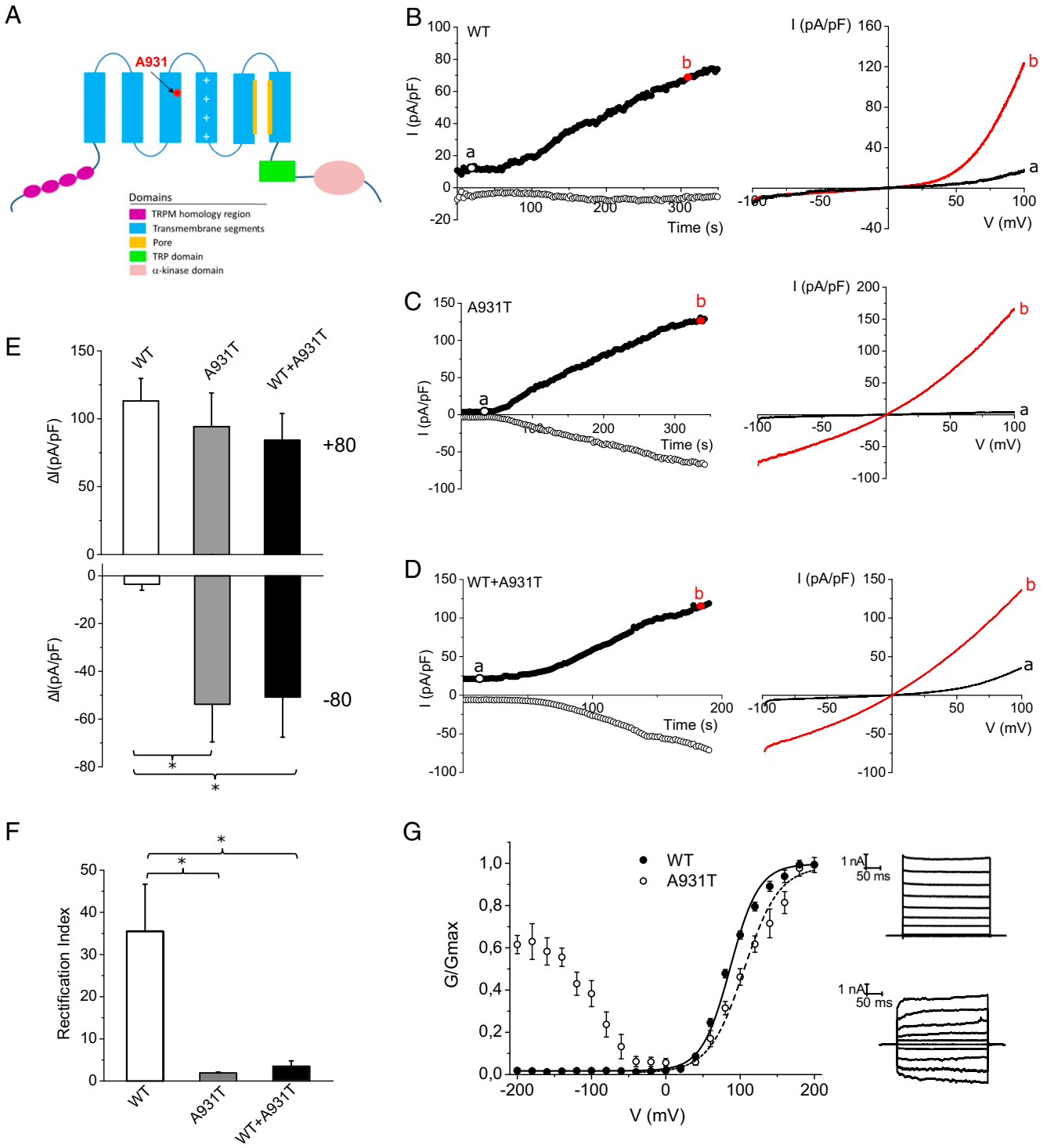

Fig. 1. A931T mutation increases TRPM7 inward current. (*A*) Location of the A931T mutation in the TRPM7 channel. Representative time courses (*Left*) at +80 mV (closed symbols) and –80 mV (open symbols) and I-V traces (*Right*) of development of TRPM7 current are shown for WT (*B*), A931T (*C*), and WT+A931T (*D*) transfected cells. The *Right* panels of *B–D* show the current-voltage relationships at the time points indicated in the *Left* panels, i.e., at break-in (<1 min after establishing whole-cell configuration) and 5 min after cell dialysis with the Mg^{2+}-free pipette solution. (*E*) Pooled data of whole-cell current at +80 mV and –80 mV evoked after cell dialysis with the Mg^{2+}-free pipette solution, from WT TRPM7 (n = 10), A931T (n = 14), and WT+A931T (n = 8) transfected cells. Each column represents mean ± SEM *P < 0.05 (one-way ANOVA). (*F*) Bar graph showing the rectification index (current amplitude ratios of +80 mV/–80 mV) of WT (n = 10), A931T (n = 14 cells), and WT+A931T (n = 8). Data are expressed as mean ± SEM *P < 0.05 (one-way ANOVA). (*G*) G-V plots of TRPM7 currents for WT and A931T. The normalized conductance (G/G_{max}) was plotted against voltage and fitted with a Boltzmann function, giving rise to 87 ± 2 mV as $V_{1/2}$ and 19 ± 2 mV as slope factor k for WT (n = 6), 105 ± 5 mV as $V_{1/2}$, and 24 ± 4 mV as k factor for A931T (n = 6). Representative currents are shown in the *Right* panel for WT (*Top*) and A931T (*Bottom*).

of TRPM7 activator Naltriben (20) on WT and A931T channels by performing patch-clamp experiments. We found that Naltriben activated a large outward current in both WT and A931T, but surprisingly it had a little effect on the inward current of A931T (*SI Appendix*, Fig. S3 *A* and *B*). We compared the effect of Naltriben on the omega current of A931T channels with its known effect on E1047Q mutant channels that generates a Na^+ inward current due to an increase in the permeability of

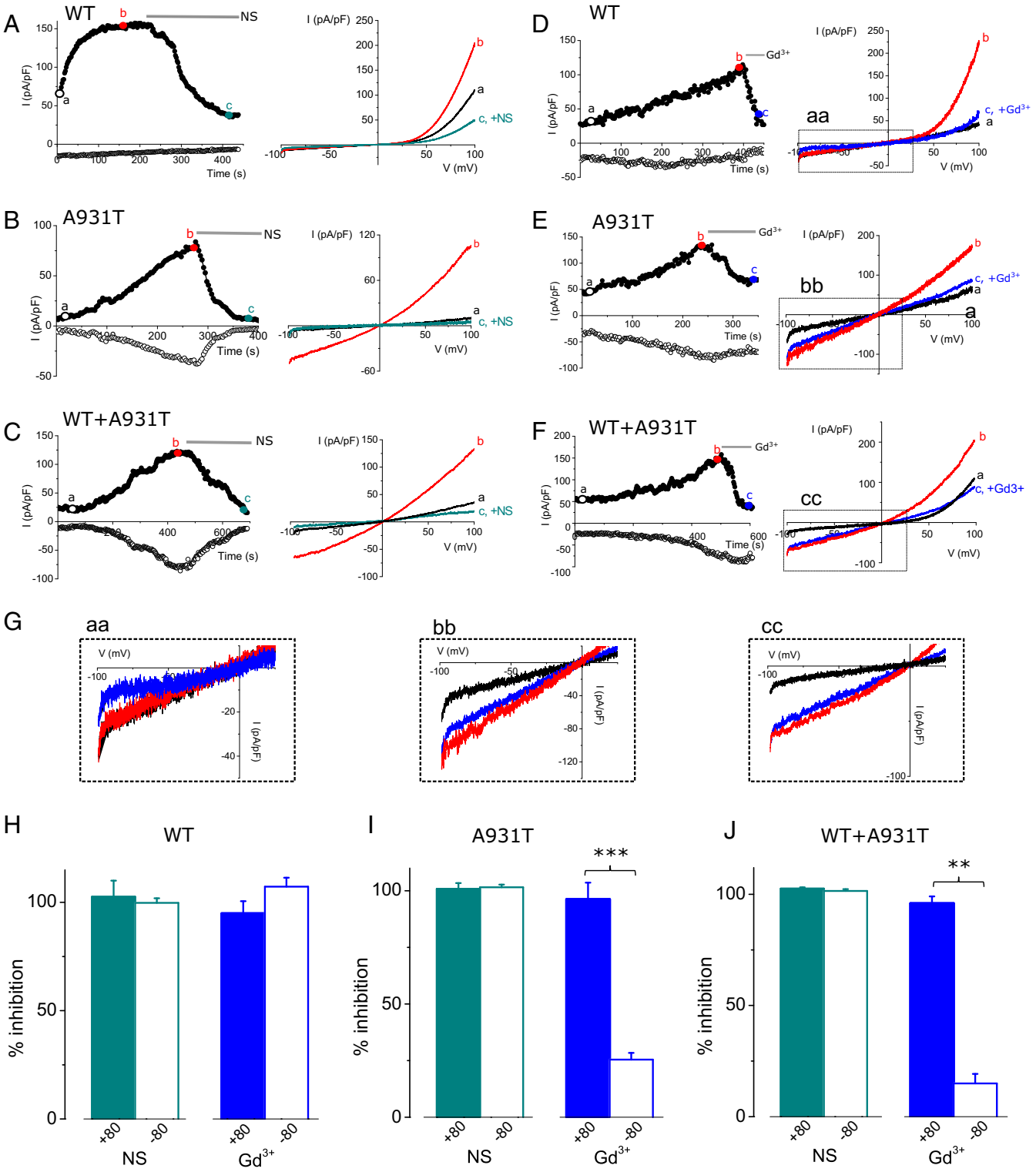

Fig. 2. A931T inward current is blocked by NS8395 but is less sensitive to Gd^{3+}. (*A–C*) Representative time courses (*Left*) and I-V traces (*Right*) of development of TRPM7 current for WT, A931T, and WT+A931T during application of TRPM7 antagonist NS8593 (NS, 10 μM). (*D–F*) Representative time courses (*Left*) and I-V traces (*Right*) of development of TRPM7 current for WT, A931T, and WT+A931T during application of Gd^{3+} (100 μM). (*G*) Enlarged view of inward currents (boxed area in *A*) in cells transfected with WT (*aa*), A931T (*bb*), and WT+A931T (*cc*) channels, in the absence and presence of Gd^{3+}. (*H*) Percentage inhibition of WT outward (+80 mV) and inward (–80 mV) currents upon application of NS8593 (green, $n = 6$) and Gd^{3+} (blue, $n = 6$). (*I*) Percentage inhibition of A931T outward (+80 mV) and inward (–80 mV) currents upon application of NS8593 (green, $n = 8$) and Gd^{3+} (blue, $n = 5$). (*J*) Percentage inhibition of WT+A931T outward (+80 mV) and inward (–80 mV) currents upon application of NS8593 (green, $n = 6$) and Gd^{3+} (blue, $n = 6$). Each column represents mean ± SEM ***$P < 0.0001$, **$P < 0.001$ (unpaired Student's t test).

monovalent cations through the canonical pore (21, 22). The Naltriben-induced increase of the inward and outward current in E1047Q channels was similar and was significantly greater than the effect on the inward current of A931T channels (*SI Appendix*, Fig. S3*C*), suggesting that Naltriben mainly activates the pore current and has little effect on the omega current.

A931T Is Not Permeable to $NMDG^+$ but Is Permeable to Guanidinium. To better characterize the biophysical properties of the inward current generated by A931T, we recorded WT and A931T currents when extracellular Na^+ was replaced with different monovalent cations. When Na^+ was substituted by guanidinium ions (Gua^+), a significantly larger inward current was observed in A931T (Fig. 3*B*) compared to WT (Fig. 3*A*). This suggests that A931T inward current was not completely selective since the gating pore leak created by A931T mutation was also permeable to guanidinium ions. However, A931T inward current had some cation specificity since it was abolished when Na^+ was replaced by $NMDG^+$ (Fig. 3 *D* and *E*), suggesting that $NMDG^+$ is too large to permeate A931T gating pore. Collectively, we interpret the effects Na^+/$NMDG^+$ substitution as evidence that the anomalous inward current generated by A931T was carried primarily by Na^+.

A931T Creates a Noncanonical Pore Permeable to Na^+ but Impermeable to Ca^{2+}. Measurements of intracellular Na^+ revealed that incubation of A931T transfected cells in Krebs solution led to a rise in Na^+ influx, whereas the $[Na]_i$ in WT cells did not increase. Moreover, the basal Na^+ was significantly higher in A931T compared to WT (0.93 ± 0.02 for WT, $n = 6$ experiments; 0.99 ± 0.01 for A931T, $n = 6$; $P < 0.05$, unpaired Student's t test), suggesting that an additional Na^+ influx was present in A931T expressing cells (*SI Appendix*, Fig. S4). In a different series of experiments, cells were initially incubated with a Na^+-free medium and Na^+ influx was measured upon change to a 140 mM Na^+ containing solution (Fig. 4*A*). A larger and statistically significant increase in Na^+ influx was observed in cells expressing A931T compared to WT-transfected cells (Fig. 4*B*).

To further delineate the role of the "omega" channel pore in the A931T channel and distinguish between the omega current of the A931T mutant channel from that of the canonical pore, we looked for mutations that differentially influence the properties of the two pores. We tested a loss-of-function mutation in the canonical pore, D1054A that regulates pH sensitivity of TRPM7 channels (22). We found that the amplitude of the outward current developed by the opening of D1054A channels after Mg^{2+} depletion was significantly lower compared to WT channels (59 ± 8 pA/pF vs. 113 ± 15 pA/pF for D1054A and WT, respectively; $P < 0.05$, unpaired Student's t test).

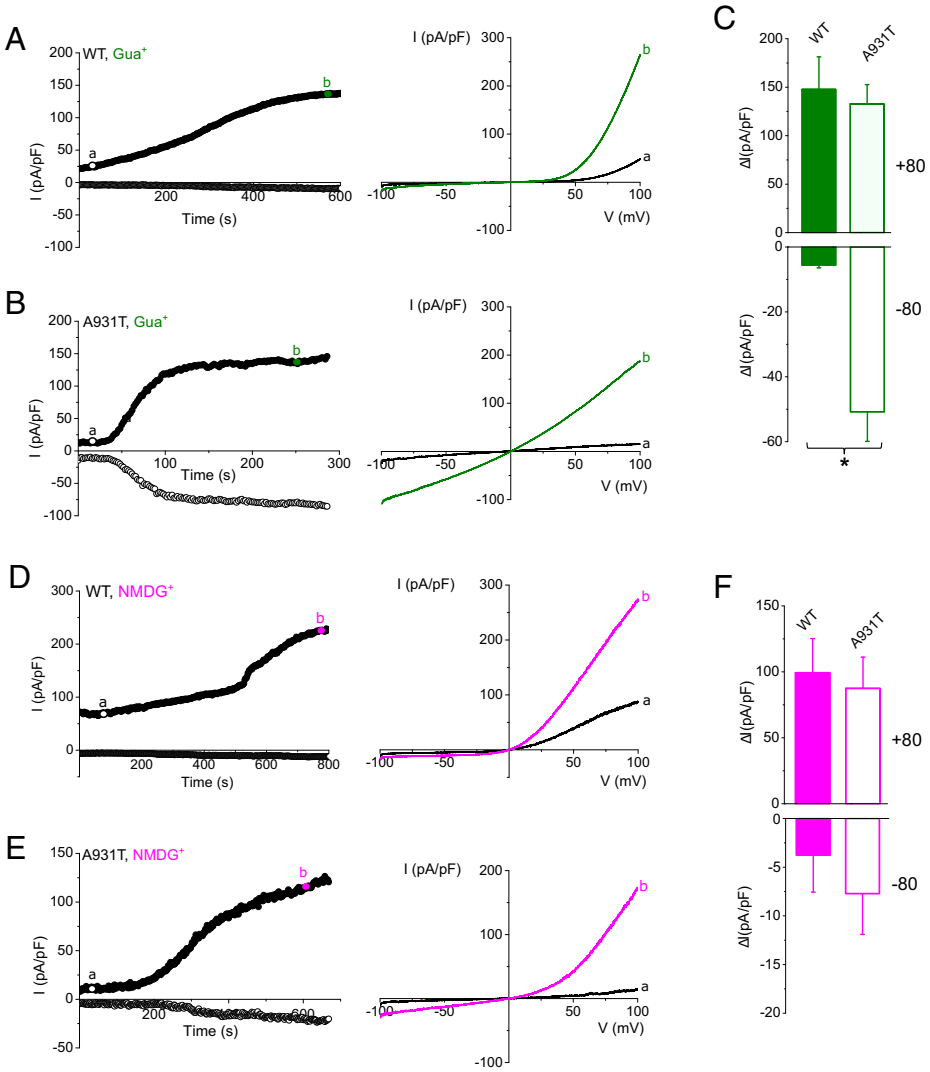

Fig. 3. A931T is permeable to Gua^+, but not to $NMDG^+$. Representative time courses (*Left*) and I-V traces (*Right*) of development of TRPM7 current in 140 mM Guanidinium (Gua^+) are shown for WT (*A*) and A931T (*B*). Pooled data of whole-cell current at +80 mV and –80 mV (*C*) from WT ($n = 6$) and A931T ($n = 6$) transfected cells. Representative time courses (*Left*) and I-V traces (*Right*) of TRPM7 current in the presence of 140 mM $NMDG^+$ are shown for WT (*D*) and A931T (*E*). Pooled data of whole-cell current at +80 mV and –80 mV (*F*) evoked after cell dialysis with the Mg^{2+}-free pipette solution, from WT ($n = 6$) and A931T ($n = 7$) transfected cells. Each column represents mean ± SEM *$P < 0.05$ (unpaired Student's t test).

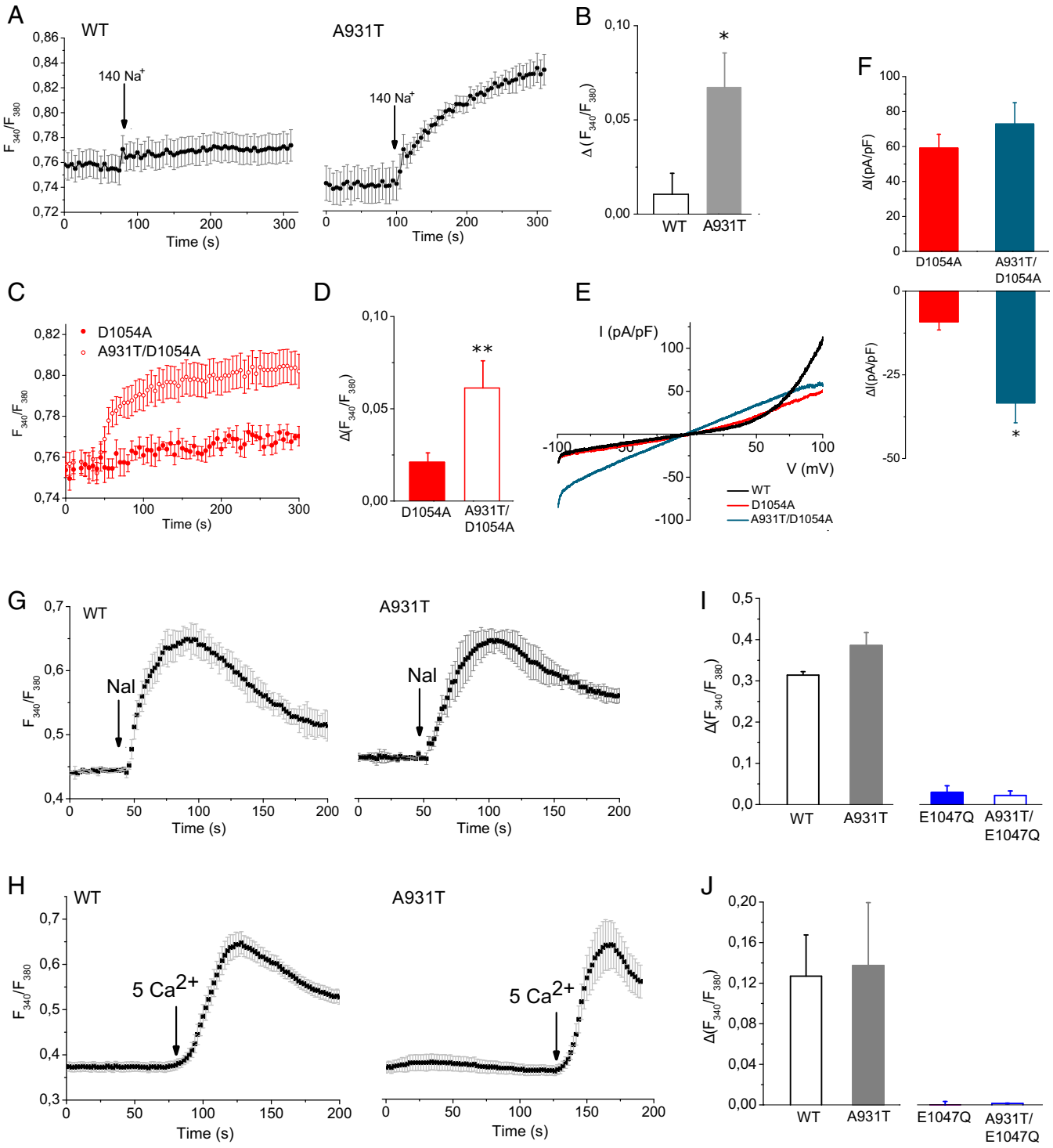

Fig. 4. A931T creates a noncanonical pore permeable to Na^+ but impermeable to Ca^{2+}. (*A*) Representative average changes in the SBFI ratio of HEK 293 cells transfected WT and A931T during replacement of extracellular 140 mM $NMDG^+$ with 140 mM Na^+. (*B*) Average increase in SBFI ratio in response to 140 mM Na^+ (n = 10 coverslips for each clone). (*C*) Representative average changes (*C*) and average increase (*D*) in the SBFI ratio of HEK 293 cells transfected with D1054A and A931T/D1054A mutants during replacement of extracellular 140 mM $NMDG^+$ with 140 mM Na^+. (*E*) Representative I-V traces of TRPM7 currents through WT, D1054A, and A931T/D1054A transfected cells. (*F*) Pooled data of whole-cell current at +80 mV and −80 mV from D1054A (n = 6) and A931T/D1054A (n = 8) transfected cells. Representative average changes in the Fura-2 ratio of HEK 293 cells transfected with WT and A931T in the presence of 50 μM Naltriben (*G*) and 5 mM Ca^{2+} (*H*). Average increase in Fura-2 ratio of HEK 293 cells transfected with WT, A931T, E1047Q, and A931T/E1047Q in response to 50 μM Naltriben (*I*, n = 10 coverslips for each clone) and 5 mM Ca^{2+} (*J*, n = 12 coverslips for each clone). Each column represents mean ± SEM $^{**}P < 0.05$, $^{*}P < 0.05$ (unpaired Student's t test).

We tested the double mutant A931T/D1054A and found that the introduction of the A931T mutation does not change the outward current, while the inward current is significantly increased (Fig. 4 *E* and *F*). Interestingly, the A931T/D1054A double mutant channel produces a significantly larger increase in Na^+ influx compared to cells expressing the single mutant D1054A channels (Fig. 4 *C* and *D*). This means that the central pore and the noncanonical pore created by A931T are distinct, and it is possible to influence the two components of the current by introducing targeted mutations.

Finally, by performing Fura-2 experiments we tested the response to TRPM7 agonist, in order to understand whether the mutation affects TRPM7 Ca^{2+} permeability leading to a gain-of-function or loss-of-function phenotype. External application of the activator naltriben evoked a fast and sustained increase of $[Ca^{2+}]_i$ in both WT and A931T (Fig. 4*G*). In a different set of experiments, Ca^{2+} influx due to TRPM7 activation was measured after increasing from 1 mM to 5 mM the concentration of Ca^{2+} in the extracellular medium (Fig. 4*H*). Comparably large increases in Ca^{2+} influx were seen in cells expressing WT or A931T mutant.

A931T induced distinctive changes in the current-voltage relationship and Na^+ permeability of TRPM7 that closely resemble the alterations shown by the E1047Q mutation (21, 22). This mutation abolishes the binding site for divalent cations in the selectivity filter of the TRPM7 channel resulting in a significant increase in Na^+ permeability through the canonical pore and produces a large inward current (*SI Appendix*, Fig. S3*C*) (20, 21). In order to distinguish the E1047Q-like effects on the canonical channel pore from the A931T omega channel pore, we performed Ca^{2+} imaging experiments on cells expressing the single mutant E1047Q and the double mutant A931T/E1047Q. Our Ca^{2+} imaging experiments showed that the E1047Q variant did not produce any detectable Ca^{2+} influx after TRPM7 activation in the presence of Naltriben or 5 mM Ca^{2+}, as consequence of the loss of divalent cation permeability due to the introduction of a neutralizing mutations (E1047Q) in the selectivity filter of TRPM7 channel. Similarly, the double mutant A931T/E1047Q did not produce any significant Ca^{2+} uptake (Fig. 4 *I* and *J*; traces are shown in *SI Appendix*, Fig. S5 *E* and *F*). Based on these experiments, we hypothesize that the Ca^{2+} uptake shown in Fig. 4 *G* and *H* is solely due to Ca^{2+} entry through the canonical channel pore, and the A931T mutation does not alter calcium permeability significantly. Furthermore, these data confirm that the omega pore generated by the A931T mutation is not permeable to Ca^{2+}.

A931T Mutation Destabilizes the Hydrophobic Ring in Proximity of the Voltage Sensor Domain. In the cryo-electron microscopy (cryo-EM) structure of hTRPM7 (22), the A931 side chain points toward the hydrophobic amino acids W972 and F971 (Fig. 5*A*), creating a hydrophobic seal between the inner and outer aqueous vestibules. We hypothesized that the replacement of the hydrophobic alanine at position 931 with the more polar threonine drastically destabilized this hydrophobic ring, thereby abolishing the seal between the two transmembrane domains and generating a Na^+ leak current.

In order to test if either the hydrophilicity of threonine or the length of its side chain play the major role in destabilizing the S3-S4 interaction, we replaced Ala931 with Ser, both amino acids having a side chain of similar size. A significantly larger inward current was observed for A931S compared to WT (Fig. 6*B*), suggesting that the introduction of a hydroxyl group in the side chain, and not the extension of the length of the side chain, was the key element for A931T gating current generation. Since A931 side chain is facing the aromatic residues F971 and W972 in S4 segments, we performed alanine substitutions of F971 and W972 in order to study their effect on channel gating. Current recordings from cells expressing F971A showed current-voltage relationships nearly similar to those recorded with WT channels. On the contrary, W972A and the double Ala mutants F971A-W972A generated a large inward current, while the amplitude of the outward current was similar (Fig. 6*B*; the statistical analysis and the RI of each clone are shown in Fig. 6*C*), suggesting a main role of A931-W972 hydrophobic interaction in S3-S4 hydrophobic cleft stability. Together, these results strongly support the idea that the introduction of Thr at position 931 disrupts the hydrophobic interactions surrounding the voltage-sensing domain and this generates a Na^+ leak current.

A931T Mutation Lowers Current Threshold and Resting Membrane Potential and Increases Evoked Firing Activity, $[Ca^{2+}]_i$ and $[Na^+]_i$ in TG Neurons. To determine whether the TRPM7 mutation A931T leads to changes in neuronal excitability, current-clamp recordings were performed on cultured TG neurons transiently transfected with WT and A931T TRPM7 plasmids. Representative action potential traces from WT and A931T TG neurons in response to depolarizing current steps showed that an action potential was elicited at a threshold of 180 pA and 80 pA, respectively (Fig. 6*A*). The resting membrane potential was significantly lower in A931T transfected neurons compared to WT neurons (WT, –53 ± 2 mV, $n = 11$; A931T, –43 ± 2 mV, $n = 8$; Fig. 6*B*). A931T mutation significantly increased the maximal number of action potentials evoked by a current stimuli of 1 s, up to 750 pA in TG neurons (Fig. 6*C*). Moreover, the mean current threshold for action potential firing in A931T transfected neurons was significantly lower compared to WT transfected TG neurons (WT, 192 ± 22 pA, $n = 11$; A931T, 110 ± 18 pA, $n = 8$; Fig. 6*D*).

We have previously shown that small depolarization of the RMP of sensory neurons increases their excitability (23–25). To assess the contribution of the A931T-induced depolarization of RMP of TG neurons on their excitability, we injected a hyperpolarizing current to hold TG neurons expressing A931T near their normal resting membrane potential of ~-55 mV. We show that evoked firing activity and threshold currents of A931T-expressing neurons that are held at ~-55 mV are similar to TG neurons expressing WT TRPM7 channels (Fig. 6 *E* and *F*). In the example shown in Fig. 6*E*, a TG neuron expressing A931T had an RMP of –44 mV and a threshold current of only 60 pA, whereas the same cell had a threshold current of 140 pA and significantly lower evoked firing activity when held at –58 mV.

Finally, the initial Fura-2 and SBFI fluorescence signal ratios, which reflect the basal intracellular $[Ca^{2+}]$ and $[Na^+]$, respectively, were significantly higher in cells expressing A931T compared to WT TRPM7 (Fig. 6 *G* and *H*). Thus, A931T resulted in depolarization and hyperexcitability of TG neurons, likely due to an increase in the intracellular basal Na^+ concentration and Ca^{2+} concentration in TG neurons.

Discussion

This study explores the potential pathogenic effects of a mutation found in the TRPM7 channel in a patient suffering from familial trigeminal neuralgia. We show that this rare mutation (A931T) results in an abnormal Na^+ influx that appears to be due to destabilization of a hydrophobic cleft between two transmembrane domains that generates a Na^+ leak current and demonstrate that expression of TRPM7 mutant channels produces trigeminal ganglion neuron depolarization and hyperexcitability.

Our data show that A931T mutation forms a pathogenic gating pore, distinct from the central pore, which was large enough to pass ions as large as guanidinium. The existence of a nonselective cation pore, the so-called omega or "gating" pore that opens in the usually nonconductive voltage sensor domains (VSD), has been described in a number of voltage-gated ion channels. A gating pore current was first described in the

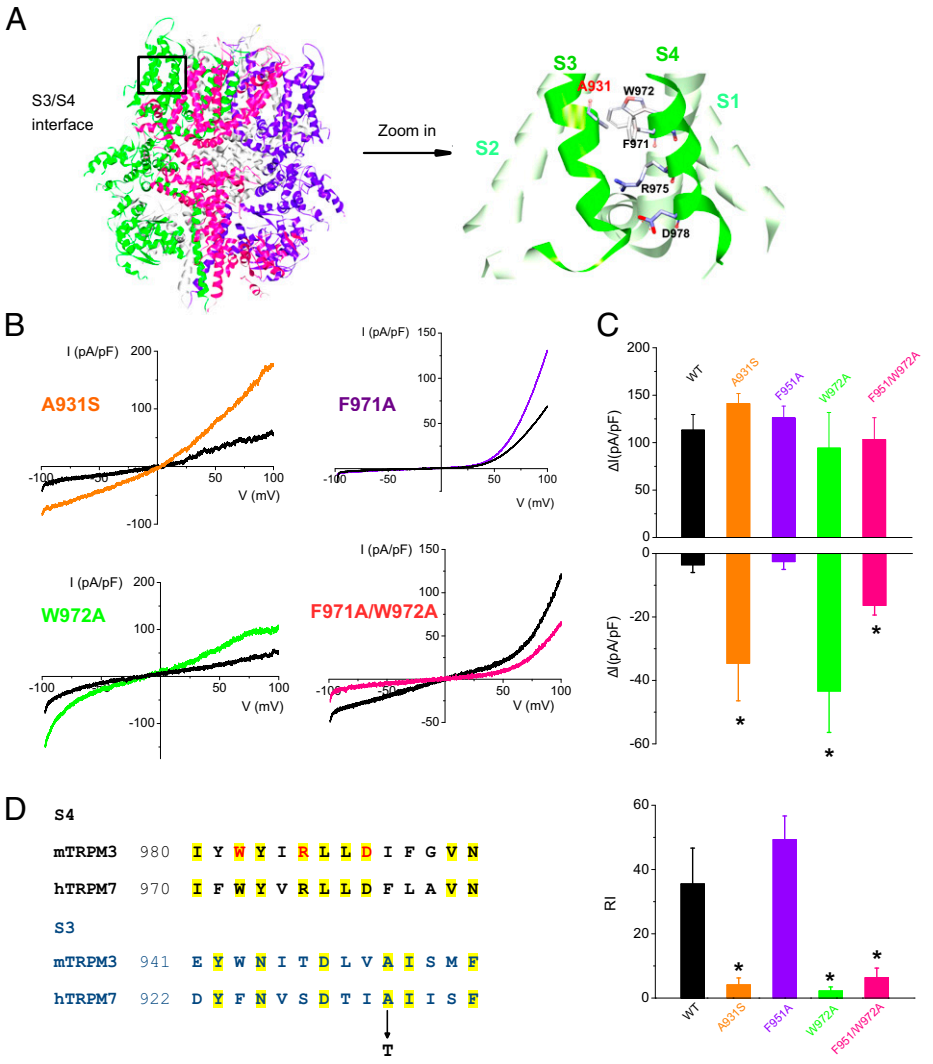

Fig. 5. A931T mutation destabilizes the hydrophobic ring in proximity of the voltage sensor domain. (*A*) Location of A931 in the TRPM7-EDTA cryo-EM structure (PDB: 5zx5). The residue corresponding to A931 is located in S3 facing the hydrophobic residues F971 and W972 and in close proximity to the charged residues R975 and D978 in the S4 voltage sensor. The image was made using BIOVIA Discovery Studio software. (*B*) Representative I-V traces of development of TRPM7 current for A931S, F971A, W972A, and F971A/W972A mutants. (*C*) Pooled data of whole-cell currents at +80 mV (*Top*) and –80 mV and RI for A931S, F971A, W972A, and F971A/W972A mutants. Each column represents mean ± SEM **P* < 0.05 vs. WT (one-way ANOVA). (*D*) Sequence alignment of transmembrane S3 and S4 of TRPM7 with TRPM3. Matched amino acids are highlighted in yellow. The residues in red play a crucial role for the existence of the alternative ion permeation pathway in TRPM3 (36). The arrow indicates the residue A931 in TRPM7.

Shaker K^+ channel, where histidine substitutions of arginine in position R1 or R4 in S4 created a proton conduction pathway distinct from the K^+-selective pore (26). Other substitutions of the first arginine in Shaker S4 by smaller amino acids produced a nonselective cation conductance that was permeable to guanidinium and was activated at hyperpolarizing potentials (27, 28). Gating pore currents generated by arginine mutations of S4 have been also described in Na_V, Ca_V, and K_V channels and some of them have been associated with channelopathies. R1 and R2 mutations in $hNa_V1.4$ (29–31) and the variants R528H and R528G in $Ca_V1.1$ (32) have been linked to hypokalemic periodic paralysis. Arginine mutations in S4 of neuronal Kv7.2 channels have been associated with benign familial neonatal seizures and peripheral nerve hyperexcitability (33). Mutation at position R1 (R219H) in the Nav1.5 channel has been linked with a case report of ventricular arrhythmias and dilated cardiomyopathy (34). Omega currents are state-dependent in that, depending on the position of the mutated gating charged residue along the transmembrane S4 helix, they can occur at hyperpolarized (closed state) or depolarized (open state) conditions (35).

Thus far, the existence of a noncanonical pore, alternative to the central pore, has been reported for only one member of the TRP channel family, the TRPM3 channel. TRPM3 displays a noncanonical pore in VSDs that can be gated by combined stimulation with pregnenolone sulfate and clotrimazole (36). Interestingly, the S4 mutation V990M of TRPM3 channel has been associated with epileptic encephalopathies, resulting in the activation of a large gating pore current via the voltage sensor domain (37).

Here, we showed that the S3 mutation A931T produced an inward current ∼20-fold higher than TRPM7 WT and this additional inward current component revealed some similarities with the TRPM3 omega currents described in (36): 1) it was produced in response to membrane hyperpolarization; 2) it was carried by Na^+ ions, and not by Ca^{2+}, under physiological conditions; 3) it was poorly sensitive to the pore blocker Gd^{3+} and to the TRPM7 agonist Naltriben; and 4) it was present when Na^+ was replaced by guanidinium, but it was completely suppressed by application of $NMDG^+$ as monovalent cation in the external solution.

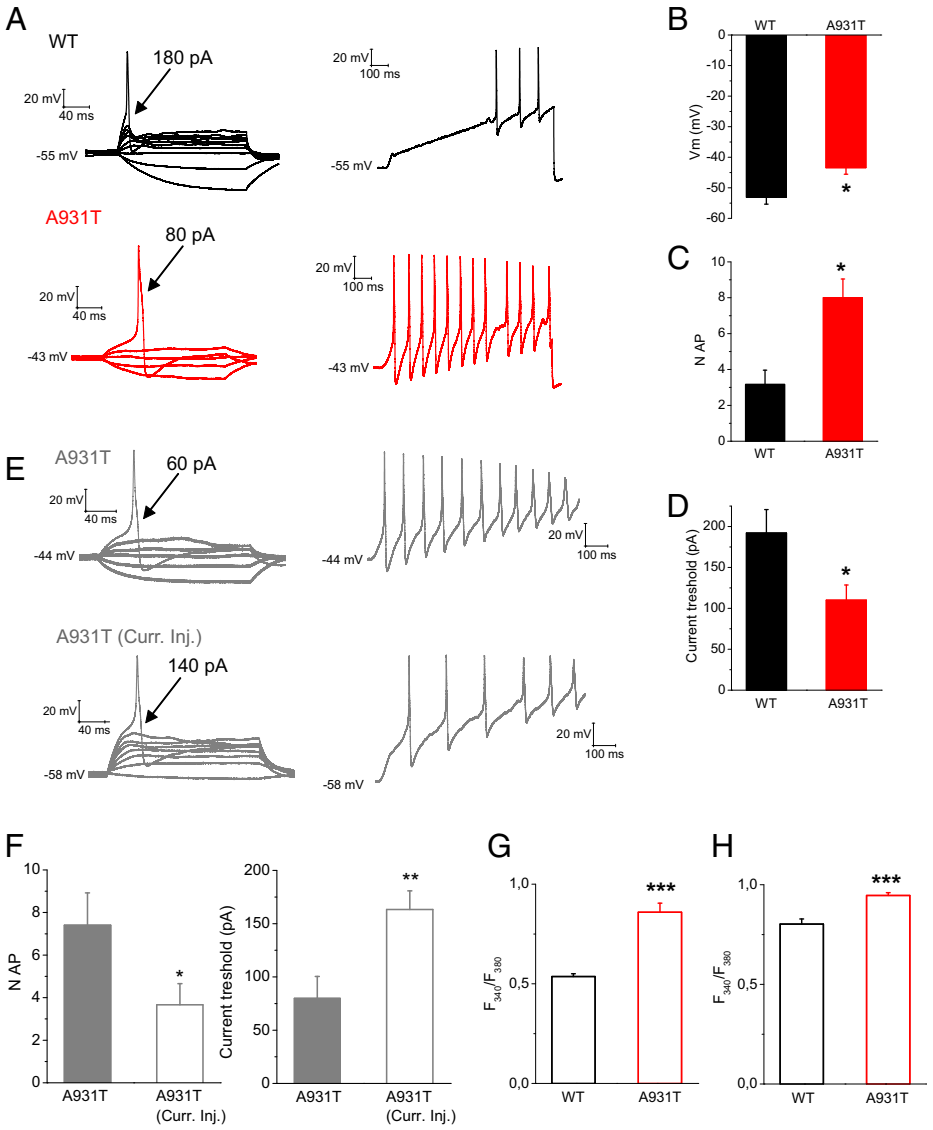

Fig. 6. A931T mutation lowers current threshold and resting membrane potential, while increasing evoked firing activity, $[Na^+]_i$ and $[Ca^{2+}]_i$ in TG neurons. (*A*) Representative traces from a WT and A931T transfected TG neuron, showing current threshold (*Left*) and action potential frequency (*Right*). Arrows indicate the current amplitude used to elicit the labeled response (180 pA for WT and 80 pA for A931T, respectively). Comparison of resting membrane potential (*B*), maximal number of action potentials evoked in response to external current stimuli of 1 s, up to 750 pA (*C*), and current threshold (*D*) in WT ($n = 11$) and A931T ($n = 8$) transfected neurons. (*E*) Representative traces from a A931T transfected TG neuron, before and after current injection to reach the same RMP as WT neurons, showing current threshold (*Left*) and action potential frequency (*Right*). Arrows indicate the current amplitude used to elicit the labeled response (60 pA for A931T and 140 pA for A931T after current injection, respectively). (*F*) Comparison of maximal number of action potentials evoked in response to external current stimuli of 1 s, up to 750 pA, and current threshold in A931T transfected neurons before and after current injection ($n = 6$). Basal Fura-2 ratio (*G*) and SBFI ratio (*H*) in WT ($n = 4$ coverslips) and A931T ($n = 4$ coverslips) transfected TG neurons. Each column represents mean ± SEM $*P < 0.05$, $***P < 0.001$ (unpaired Student's *t* test).

The residue A931 is located in the S3 segment, at the interface with the voltage-sensing transmembrane region S4 (Fig. 5*A*). The residues W982, R985, and D988 in S4 play a crucial role for the existence of the alternative ion permeation pathway in TRPM3 (38). Sequence alignment (Fig. 5*D*) of the S3 and S4 transmembrane domains of TRPM7 and TRPM3 channels showed a high level of homology between the two channels, with the three amino acids W982, R985, and D988 in S4 of TRPM3 being conserved and equivalent to W972, R975, and D978 in TRPM7. This may suggest similar interactions between S3 and S4 domains in the two channels.

One point that still needs to be clarified regarding the formation of an omega pore through the VSD of TRPM7 is whether the mutation A931 in S3 reveals a cryptic gating-charge pore through the VSD as the one described for TRPM3 or whether the mutation simply destabilizes and compromises the impermeability of the VSD resulting in ionic leak.

As noted above, gating pores are usually caused by mutations of S4 positively charged amino acids that create a misalignment of the S4 voltage-sensing residues and the narrow hydrophobic cleft through which the S4 helix translocate during voltage-dependent movements, thus abolishing the seal between the outer hydrophilic vestibule and the cytoplasmic compartment. However, mutations of the hydrophobic non-voltage-sensing amino acids located around the positive charges of S4 (the so-called "hydrophobic plug") may have also a significant effect on channel gating (39, 40). For example, several hydrophobic amino acids located near S4 in the Shaker K^+ channel when mutated contribute to the generation of gating currents (I237 on S1, F290 on S2) (41) or catalyze the gating charge transfer during conformational dynamics of voltage sensors (42); mutations of hydrophobic amino acids in the voltage-sensing domain of Hv1 channel produces gating pore currents (39). In this study, we showed that the replacement of the hydrophobic

alanine at position 931 with the more polar threonine drastically destabilizes the interaction between S3 and S4, possibly suggesting that this residue is part of the hydrophobic plug that separates the water-accessible crevices in TRPM7.

In addition to promoting an omega current, A931T mutation affects the voltage sensitivity of the central pore current. It has been previously demonstrated that hydrophobic mutations near the segment S4 shift steady-state activation and/or inactivation curves of Shaker K^+ channel (43). Moreover, mutations of amino acids predicted to face the sensor domain cavity of TRPA1 dramatically alter the voltage-dependent activation properties of the channels (44). Our results show that A931T affects the open-closed equilibrium of TRPM7, significantly decreasing the activation probability, as indicated by an ~15 mV depolarizing shift of G/V midpoint.

In summary, our results demonstrate that mutation A931T in TRPM7, found in a patient with familial trigeminal neuralgia and located in the S3 segment of the channel at the interface with the voltage-sensing S4 region, produces dramatic changes of TRPM7 channel properties. These changes include a 20-fold increase in inward currents that appears to be due to destabilization of a hydrophobic ring near the voltage sensor domain. Our results show that A931 channels generate an omega current that carries a sustained Na^+ influx under physiological conditions. When studied at the cellular level within trigeminal ganglion neurons, the A931T mutation produces changes in resting membrane potential, current threshold, and repetitive firing that likely contribute to the abnormal firing that has been identified as a contributor to pain in trigeminal neuralgia (4–6). Thus, in addition to our demonstration that a mutation in a TRPM7 channel can produce an omega current, our results indicate that this mutation contributes to pain in this kindred with familial trigeminal neuralgia.

Materials and Methods

HEK 293 cells were transiently transfected with vectors that encode human TRPM7 and A931T, A931S, F971A, W972A, F971A/W972A, E1047Q, D1054A, A931T/E1047Q, and A931T/D1054A mutants. Patch-clamp studies and Na^+ and Ca^{2+} imaging experiments were carried out as previously described (8). The WT TRPM7 plasmid was obtained from Genescript, in which the insert was cloned in-frame with 2A-GFP at the C terminus of the channel in the vector pcDNA3.1 (45, 46). Transfection of TG neurons was performed as previously described (47). Complete details are described in *SI Appendix*.

Data, Materials, and Software Availability. All study data are included in the article and/or *SI Appendix*.

ACKNOWLEDGMENTS. We thank Fadia B. Dib-Hajj and Daniel Sosniak for technical assistance. This work was supported by funding from the Rehabilitation Research Service and Biomedical Laboratory Research Service, Department of Veterans Affairs.

1. G. Cruccu, G. Di Stefano, A. Truini, Trigeminal neuralgia. *N. Engl. J. Med.* **383**, 754–762 (2020).
2. A. L. Ko *et al.*, Trigeminal neuralgia without neurovascular compression presents earlier than trigeminal neuralgia with neurovascular compression. *J. Neurosurg.* **123**, 1519–1527 (2015).
3. S. Panchagnula, A. K. Sularz, K. T. Kahle, Familial trigeminal neuralgia cases implicate genetic factors in disease pathogenesis. *JAMA Neurol.* **76**, 9–10 (2019).
4. K. J. Burchiel, Ectopic impulse generation in focally demyelinated trigeminal nerve. *Exp. Neurol.* **69**, 423–429 (1980).
5. M. Devor, R. Amir, Z. H. Rappaport, Pathophysiology of trigeminal neuralgia: The ignition hypothesis. *Clin. J. Pain* **18**, 4–13 (2002).
6. H. Z. Rappaport, M. Devor, Trigeminal neuralgia: The role of self-sustaining discharge in the trigeminal ganglion. *Pain* **56**, 127–138 (1994).
7. G. Di Stefano *et al.*, Familial trigeminal neuralgia–A systematic clinical study with a genomic screen of the neuronal electrogenisome. *Cephalalgia* **40**, 767–777 (2020).
8. R. Gualdani *et al.*, Trigeminal neuralgia TRPM8 mutation: Enhanced activation, basal $[Ca^{2+}]_i$ and menthol response. *Neurol. Genet.* **7**, e550 (2021).
9. I. Vandewauw, G. Owsianik, T. Voets, Systematic and quantitative mRNA expression analysis of TRP channel genes at the single trigeminal and dorsal root ganglion level in mouse. *BMC Neurosci.* **14**, 21 (2013).
10. A. Fleig, V. Chubanov, TRPM7. *Handb. Exp. Pharmacol.* **222**, 521–546 (2014).
11. V. Chubanov, L. Mittermeier, T. Gudermann, Role of kinase-coupled TRP channels in mineral homeostasis. *Pharmacol. Ther.* **184**, 159–176 (2018).
12. L. V. Ryazanova *et al.*, TRPM7 is essential for Mg(2+) homeostasis in mammals. *Nat. Commun.* **1**, 109 (2010).
13. J. Jin *et al.*, The channel kinase, TRPM7, is required for early embryonic development. *Proc. Natl. Acad. Sci. U.S.A.* **109**, E225–E233 (2012).
14. L. Mittermeier *et al.*, TRPM7 is the central gatekeeper of intestinal mineral absorption essential for postnatal survival. *Proc. Natl. Acad. Sci. U.S.A.* **116**, 4706–4715 (2019).
15. M. K. Monteilh-Zoller *et al.*, TRPM7 provides an ion channel mechanism for cellular entry of trace metal ions. *J. Gen. Physiol.* **121**, 49–60 (2003).
16. M. J. Nadler *et al.*, LTRPC7 is a Mg.ATP-regulated divalent cation channel required for cell viability. *Nature* **411**, 590–595 (2001).
17. V. Chubanov *et al.*, Natural and synthetic modulators of SK (K(ca)2) potassium channels inhibit magnesium-dependent activity of the kinase-coupled cation channel TRPM7. *Br. J. Pharmacol.* **166**, 1357–1376 (2012).
18. Y. A. Ermakov, K. Kamaraju, K. Sengupta, S. Sukharev, Gadolinium ions block mechanosensitive channels by altering the packing and lateral pressure of anionic lipids. *Biophys. J.* **98**, 1018–1027 (2010).
19. A. Leffler, R. M. Linte, C. Nau, P. Reeh, A. Babes, A high-threshold heat-activated channel in cultured rat dorsal root ganglion neurons resembles TRPV2 and is blocked by gadolinium. *Eur. J. Neurosci.* **26**, 12–22 (2007).
20. T. Hofmann *et al.*, Activation of TRPM7 channels by small molecules under physiological conditions. *Pflugers Arch.* **466**, 2177–2189 (2014).
21. M. Li *et al.*, Molecular determinants of Mg^{2+} and Ca^{2+} permeability and pH sensitivity in TRPM6 and TRPM7. *J. Biol. Chem.* **282**, 25817–25830 (2007).
22. J. Duan *et al.*, Structure of the mammalian TRPM7, a magnesium channel required during embryonic development. *Proc. Natl. Acad. Sci. U.S.A.* **115**, E8201–E8210 (2018).
23. J. Huang *et al.*, Sodium channel NaV1.9 mutations associated with insensitivity to pain dampen neuronal excitability. *J. Clin. Invest.* **127**, 2805–2814 (2017).
24. J. Huang *et al.*, Atypical changes in DRG neuron excitability and complex pain phenotype associated with a $Na_v1.7$ mutation that massively hyperpolarizes activation. *Sci. Rep.* **8**, 1811 (2018).
25. M. A. Mis *et al.*, Resilience to pain: A peripheral component identified using induced pluripotent stem cells and dynamic clamp. *J. Neurosci.* **39**, 382–392 (2019).
26. D. M. Starace, E. Stefani, F. Bezanilla, Voltage-dependent proton transport by the voltage sensor of the Shaker K+ channel. *Neuron* **19**, 1319–1327 (1997).
27. F. Tombola, M. M. Pathak, E. Y. Isacoff, Voltage-sensing arginines in a potassium channel permeate and occlude cation-selective pores. *Neuron* **45**, 379–388 (2005).
28. F. Tombola, M. M. Pathak, P. Gorostiza, E. Y. Isacoff, The twisted ion-permeation pathway of a resting voltage-sensing domain. *Nature* **445**, 546–549 (2007).
29. S. Sokolov, T. Scheuer, W. A. Catterall, Gating pore current in an inherited ion channelopathy. *Nature* **446**, 76–78 (2007).
30. A. F. Struyk, S. C. Cannon, A Na+ channel mutation linked to hypokalemic periodic paralysis exposes a proton-selective gating pore. *J. Gen. Physiol.* **130**, 11–20 (2007).
31. A. F. Struyk, V. S. Markin, D. Francis, S. C. Cannon, Gating pore currents in DIIS4 mutations of NaV1.4 associated with periodic paralysis: Saturation of ion flux and implications for disease pathogenesis. *J. Gen. Physiol.* **132**, 447–464 (2008).
32. F. Wu, M. Quinonez, M. DiFranco, S. C. Cannon, Stac3 enhances expression of human $Ca_V1.1$ in *Xenopus* oocytes and reveals gating pore currents in HypoPP mutant channels. *J. Gen. Physiol.* **150**, 475–489 (2018).
33. F. Miceli, E. Vargas, F. Bezanilla, M. Taglialatela, Gating currents from Kv7 channels carrying neuronal hyperexcitability mutations in the voltage-sensing domain. *Biophys. J.* **102**, 1372–1382 (2012).
34. P. Gosselin-Badaroudine *et al.*, A proton leak current through the cardiac sodium channel is linked to mixed arrhythmia and the dilated cardiomyopathy phenotype. *PLoS One* **7**, e38331 (2012).
35. A. Moreau, P. Gosselin-Badaroudine, M. Chahine, Biophysics, pathophysiology, and pharmacology of ion channel gating pores. *Front. Pharmacol.* **5**, 53 (2014).
36. J. Vriens *et al.*, Opening of an alternative ion permeation pathway in a nociceptor TRP channel. *Nat. Chem. Biol.* **10**, 188–195 (2014).
37. E. Van Hoeymissen *et al.*, Gain of channel function and modified gating properties in TRPM3 mutants causing intellectual disability and epilepsy. *eLife* **9**, e57190 (2020).
38. K. Held *et al.*, Mutations in the voltage-sensing domain affect the alternative ion permeation pathway in the TRPM3 channel. *J. Physiol.* **596**, 2413–2432 (2018).
39. R. Banh *et al.*, Hydrophobic gasket mutation produces gating pore currents in closed human voltage-gated proton channels. *Proc. Natl. Acad. Sci. U.S.A.* **116**, 18951–18961 (2019).
40. J. L. Carvalho-de-Souza, F. Bezanilla, Nonsensing residues in S3-S4 linker's C terminus affect the voltage sensor set point in K^+ channels. *J. Gen. Physiol.* **150**, 307–321 (2018).
41. F. V. Campos, B. Chanda, B. Roux, F. Bezanilla, Two atomic constraints unambiguously position the S4 segment relative to S1 and S2 segments in the closed state of Shaker K channel. *Proc. Natl. Acad. Sci. U.S.A.* **104**, 7904–7909 (2007).
42. J. J. Lacroix, H. C. Hyde, F. V. Campos, F. Bezanilla, Moving gating charges through the gating pore in a Kv channel voltage sensor. *Proc. Natl. Acad. Sci. U.S.A.* **111**, E1950–E1959 (2014).
43. G. A. Lopez, Y. N. Jan, L. Y. Jan, Hydrophobic substitution mutations in the S4 sequence alter voltage-dependent gating in Shaker K+ channels. *Neuron* **7**, 327–336 (1991).
44. L. Zimova *et al.*, Intracellular cavity of sensor domain controls allosteric gating of TRPA1 channel. *Sci. Signal.* **11**, eaan8621 (2018).
45. J. F. Atkins *et al.*, A case for "StopGo": Reprogramming translation to augment codon meaning of GGN by promoting unconventional termination (Stop) after addition of glycine and then allowing continued translation (Go). *RNA* **13**, 803–810 (2007).
46. G. A. Luke *et al.*, Occurrence, function and evolutionary origins of '2A-like' sequences in virus genomes. *J. Gen. Virol.* **89**, 1036–1042 (2008).
47. S. D. Dib-Hajj *et al.*, Transfection of rat or mouse neurons by biolistics or electroporation. *Nat. Protoc.* **4**, 1118–1126 (2009).